

Hydrothermal synthesis and nonvolatile resistive switching properties of α-Fe_2O_3 nanosheet arrays

Zhi-Qiang Yu(余志强), Xin-Wei Zhao(赵新为), Bao-Sheng Liu(刘宝生), Tang-You Sun(孙堂友), and Zhi-Mou Xu(徐智谋)

Citation: Chin. Phys. B, 2026, 35 (**1**): 017302. DOI: 10.1088/1674-1056/adee88
http://cpb.iphy.ac.cn; http://iopscience.iop.org/cpb

What follows is a list of articles you may be interested in

Sol-gel synthesis and nonvolatile resistive switching behaviors of wurtzite phase ZnO nanofilms

Zhi-Qiang Yu(余志强), Jin-Hao Jia(贾金皓), Mei-Lian Ou(欧梅莲), Tang-You Sun(孙堂友), and Zhi-Mou Xu(徐智谋)

Chin. Phys. B, 2025, 34 (**12**): 127302. DOI: 10.1088/1674-1056/ade1c2

Nonvolatile ferroelectric control of electronic properties of Bi_2Te_3

Xusheng Ding(丁旭升), Yunfei Li(李云飞), Chaoyang Kang(康朝阳), Ye-Heng Song(宋业恒), and Weifeng Zhang(张伟风)

Chin. Phys. B, 2024, 33 (**11**): 117301. DOI: 10.1088/1674-1056/ad7670

Effects of oxygen vacancy concentration and temperature on memristive behavior of $SrRuO_3$/Nb:$SrTiO_3$ junctions

Zhi-Cheng Wang(王志成), Zhang-Zhang Cui(崔璋璋), Hui Xu(徐珲), Xiao-Fang Zhai(翟晓芳), Ya-Lin Lu(陆亚林)

Chin. Phys. B, 2019, 28 (**8**): 087303. DOI: 10.1088/1674-1056/28/8/087303

Selective enhancement of green upconversion luminescence of Er-Yb: $NaYF_4$ by surface plasmon resonance of $W_{18}O_{49}$ nanoflowers and applications in temperature sensing

Ang Li(李昂), Jin-Lei Wu(吴金磊), Xue-Song Xu(许雪松), Yang Liu(刘洋), Ya-Nan Bao(包亚男), Bin Dong(董斌)

Chin. Phys. B, 2018, 27 (**9**): 097301. DOI: 10.1088/1674-1056/27/9/097301

Flexible electrically pumped random lasing from ZnO nanowires based on metal-insulator-semiconductor structure

Miao-Ling Que(阙妙玲), Xian-Di Wang(王贤迪), Yi-Yao Peng(彭轶瑶), Cao-Feng Pan(潘曹峰)

Chin. Phys. B, 2017, 26 (**6**): 067301. DOI: 10.1088/1674-1056/26/6/067301

Hydrothermal synthesis and nonvolatile resistive switching properties of α-Fe_2O_3 nanosheet arrays

Zhi-Qiang Yu(余志强)[1,2,3,†], Xin-Wei Zhao(赵新为)[1], Bao-Sheng Liu(刘宝生)[1], Tang-You Sun(孙堂友)[4], and Zhi-Mou Xu(徐智谋)[3,‡]

[1] *School of Electronic Engineering, Guangxi University of Science and Technology, Liuzhou* 545006, *China*
[2] *School of Computer and Information Technology, Hohhot Minzu College, Hohhot* 010051, *China*
[3] *Wuhan National Laboratory for Optoelectronics, School of Optical and Electronic Information, Huazhong University of Science and Technology, Wuhan* 430074, *China*
[4] *Guangxi Key Laboratory of Precision Navigation Technology and Application, Guilin University of Electronic Technology, Guilin* 541004, *China*

(Received 30 March 2025; revised manuscript received 28 June 2025; accepted manuscript online 11 July 2025)

A facile one-step hydrothermal method has been reported to synthesize the α-Fe_2O_3 nanosheet arrays with the preferred orientation along the [104] direction on the ITO substrate. The α-Fe_2O_3 nanosheet arrays-based W/α-Fe_2O_3/ITO memristor has been achieved by depositing the circular W top electrodes on the α-Fe_2O_3 nanosheet arrays. The as-prepared W/α-Fe_2O_3/ITO memristor shows a reliable nonvolatile bipolar resistive switching behavior with the high resistance ratio of about 10^3 at the reading voltage of 0.1 V, good resistance retention over 10^3 s, ultralow set voltage of -0.6 V and reset voltage of 0.7 V, and good durability. In addition, the tunneling conduction mechanism modified by the oxygen vacancies has been proposed and suggested to be responsible for the nonvolatile resistive switching behavior of the as-prepared W/α-Fe_2O_3/ITO memristor. This work demonstrates that the as-prepared α-Fe_2O_3 nanosheet arrays-based W/α-Fe_2O_3/ITO memristor would be a promising candidate for further ultralow power nonvolatile memory applications.

Keywords: hydrothermal method, α-Fe_2O_3 nanosheet arrays, nonvolatile, tunneling conduction mechanism, oxygen vacancies

PACS: 73.40.Rw, 72.60.+g, 72.80.Ga

DOI: 10.1088/1674-1056/adee88 **CSTR:** 32038.14.CPB.adee88

1. Introduction

The memristor is usually a "sandwich" structure consisting of the resistive layer, the top and bottom electrodes, which has been regarded as the fourth fundamental circuit element due to its excellent advantages in terms of the excellent storage capacity, low power consumption, high endurance, and the ability to be compatible with the complementary metal–oxide–semiconductor (CMOS) process.[1–10] Therefore, the increasing attention has been devoted to the memristors, which have demonstrated great application potential in the aspects of information storage, logical operations, and brain-like neuromorphic computing. However, as a new type of circuit element, the internal resistive switching mechanism of the memristor still remains mysterious.

In the last decade, there have been many kinds of resistive layer materials including the inorganic and organic dielectric materials that were used for memristor applications. As the typical inorganic materials, the transition metal oxides, including the Al_2O_3,[11,12] CeO_2,[13] TaO_x,[14] CuO_2,[15–17] GaO_x,[18,19] HfO_2,[10,20–22] MnO_2,[23] NiO,[24] TiO_2,[3–8,25–29] VO_2,[30] WO_3,[9,31] ZrO_2,[29,32] ZnO,[2,33,34] and Fe_2O_3[35–50] have received great attention due to their simple structure, low cost, which are compatible with the COMS process and become the focus of the memristor applications. Among them, the hematite (α-Fe_2O_3) has shown these advantages such as the narrow band gap, excellent photoelectric properties, high chemical stability, low cost, and high natural abundance,[38] which has become an excellent candidate material for memristor applications. In recent years, many preparation methods regarding the ultrasonic spray pyrolysis,[35] hydrothermal process,[45,49] dipcoating method,[38,39,42,47,48] magnetron sputtering,[36,43] spin-coating method,[35,37,40,44,46] and the atomic layer deposition[50] have been adopted to prepare the α-Fe_2O_3. In particular, the hydrothermal process has attracted extensive attention because of its low cost, simple process, low power consumption, and relatively mild reaction conditions.[45,49] The hydrothermal process is a high-efficiency method for the controlled large-scale synthesis of the α-Fe_2O_3 nanomaterials, which has been widely utilized to prepare the various α-Fe_2O_3 nanomaterials-based devices. However, the direct hydrothermal synthesis of the α-Fe_2O_3 nanosheet arrays on the ITO substrate has never been reported and the nonvolatile resistive switching mechanism of the α-Fe_2O_3 nanosheet arrays-based W/α-Fe_2O_3/ITO memristor is still unclear so far.

[†]Corresponding author. E-mail: zhiqiangyu@alumni.hust.edu.cn
[‡]Corresponding author. E-mail: xuzhimou@mail.hust.edu.cn

© 2026 Chinese Physical Society and IOP Publishing Ltd. All rights, including for text and data mining, AI training, and similar technologies, are reserved.

In this work, a facile one-step hydrothermal process has been carried out to synthesize the α-Fe_2O_3 nanosheet arrays with a preferred growth orientation along the [104] direction on the ITO substrate. The α-Fe_2O_3 nanosheet arrays-based W/α-Fe_2O_3/ITO memristor has been achieved by depositing the circular W electrodes on the α-Fe_2O_3 nanosheet arrays. The as-prepared W/α-Fe_2O_3/ITO memristor demonstrated the nonvolatile bipolar resistive switching behavior with a high resistive switching ratio, good resistance retention ability, low set voltage and reset voltage. Moreover, the tunneling conduction mechanism modified by the oxygen vacancies has been proposed to understand the nonvolatile resistive switching properties of the as-prepared W/α-Fe_2O_3/ITO memristor. This work demonstrates that the as-prepared α-Fe_2O_3 nanosheet arrays-based W/α-Fe_2O_3/ITO memristor may be a potential candidate for the further ultralow power nonvolatile memory applications.

2. Experimental details

All the chemical agents used for the preparation of α-Fe_2O_3 nanosheet arrays are the potassium ferrocyanide ($K_4[Fe(CN)_2]\cdot 3H_2O$, purity $> 99.5\%$) as well as deionized water. All the reagents are analytically pure and not getting further treatment before use. The indium tin oxide (ITO) bottom electrode of the as-prepared W/α-Fe_2O_3/ITO memristor and the potassium ferrocyanide were purchased commercially from the NSG Pilkington and Sigma-Aldrich, respectively. The preparation process flow of the α-Fe_2O_3 nanosheet arrays-based W/α-Fe_2O_3/ITO memristor has been shown in Fig. 1.

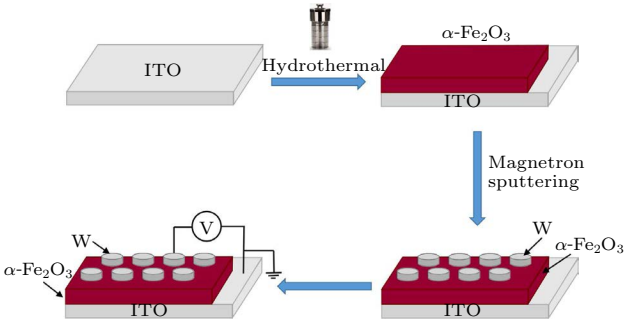


Fig. 1. Preparation process flow of the W/α-Fe_2O_3/ITO memristor.

It is clearly shown that the α-Fe_2O_3 nanosheet arrays were prepared by a facile one-step hydrothermal method. First, 0.3-mM potassium ferrocyanide was dissolved in 15 mL of deionized water and stirred magnetically for 10 min at 600 rpm. Then the solution was transferred to an autoclave, where a piece of ITO conductive glass was placed diagonally in the autoclave with the conductive side facing downward. Subsequently, the autoclave was sealed and heated at 200 °C for 6 h in a muffle furnace. After that the autoclave was cooled to room temperature naturally, the sample was removed out and rinsed with the deionized water and alcohol in turn. Finally, the circular W top electrodes with a diameter of about 5 μm were deposited on the as-prepared α-Fe_2O_3 nanosheet arrays via using magnetron sputtering and the α-Fe_2O_3 nanosheet arrays-based W/α-Fe_2O_3/ITO memristor has been prepared.

The crystal structures of the as-prepared samples were analyzed by the x-ray diffraction (XRD, PANalytical PW3040/60), in which the x-rays used Cu $K\alpha$ radiation with a wavelength of 0.1542 nm at 40 kV and 200 mA. The field emission scanning electron microscope (FESEM, FEI Nova NanoSEM450) was used to measure the morphologies of the as-prepared samples. The surface elemental compositions and chemical states of the as-prepared samples were identified by the x-ray photoelectron spectrometer (XPS, AXIS-ULTRA DLD-600W) with a monochromatic Al $K\alpha$ x-ray source and the instrument back bottom vacuum of not less than 1×10^{-7} Pa. The current–voltage (I–V) characteristics of as-prepared α-Fe_2O_3 nanosheet arrays-based W/α-Fe_2O_3/ITO memristor were explored by using an Agilent B2901A source meter under ambient temperature and pressure. During the measurement, the bias voltage was applied to the circular W top electrode of the as-prepared W/α-Fe_2O_3/ITO memristor with the grounded ITO bottom electrode to test the electrical properties of the as-prepared α-Fe_2O_3 nanosheet arrays-based W/α-Fe_2O_3/ITO memristor.

3. Results and discussion

3.1. Physical characterizations

Figures 2(a)–2(c) exhibit the top-view FESEM images of the as-prepared α-Fe_2O_3 nanosheet arrays grown on the ITO substrate under different magnifications, respectively. As shown in Figs. 2(a)–2(c), the entire surface of the ITO substrate is covered very uniformly by the nanosheet-like α-Fe_2O_3 arrays.

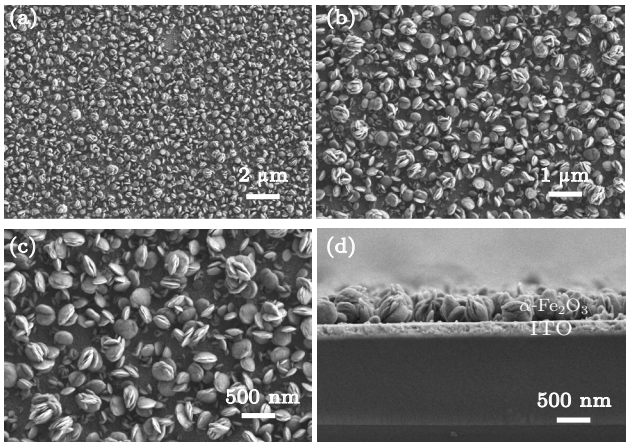


Fig. 2. Morphologies of the as-prepared samples: (a)–(c) top-view FESEM images under different magnifications, and (d) cross-sectional view FESEM image.

Figure 2(d) displays the cross-sectional view FESEM image of the as-prepared α-Fe_2O_3 nanosheet arrays. It is obvious that the thickness of the as-prepared α-Fe_2O_3 nanosheet arrays is about 500 nm. Figure 3 shows the XRD patterns of the ITO substrate and the as-prepared α-Fe_2O_3 nanosheet arrays sample grown on the ITO substrate, respectively. It is found that all the diffraction peaks that appear upon nanosheet arrays growth are classified as the rhombohedral phase α-Fe_2O_3 (PDF# 33-0664, JCPDS).[51,52] Furthermore, only the three diffraction peaks positioned at 24.2°, 33.1°, and 54.0° corresponding to the (012), (104), and (116) crystal planes of the rhombohedral phase α-Fe_2O_3 can be observed clearly from the as-prepared α-Fe_2O_3 nanosheet arrays sample, respectively. In particular, the (104) diffraction peak that appeared at 33.1° is significantly enhanced compared with the other diffraction peaks of the (012) and (116) crystal planes, suggesting that the as-prepared α-Fe_2O_3 nanosheet arrays can be grown preferentially along the [104] direction on the ITO substrate.

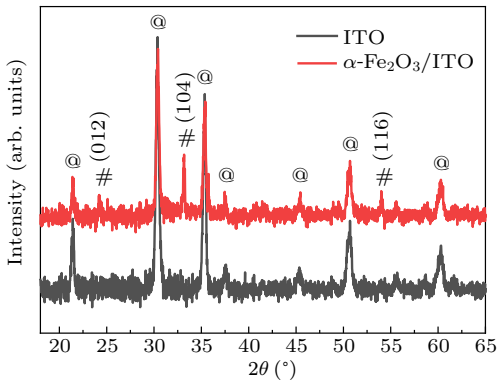


Fig. 3. XRD patterns of α-Fe_2O_3 and ITO.

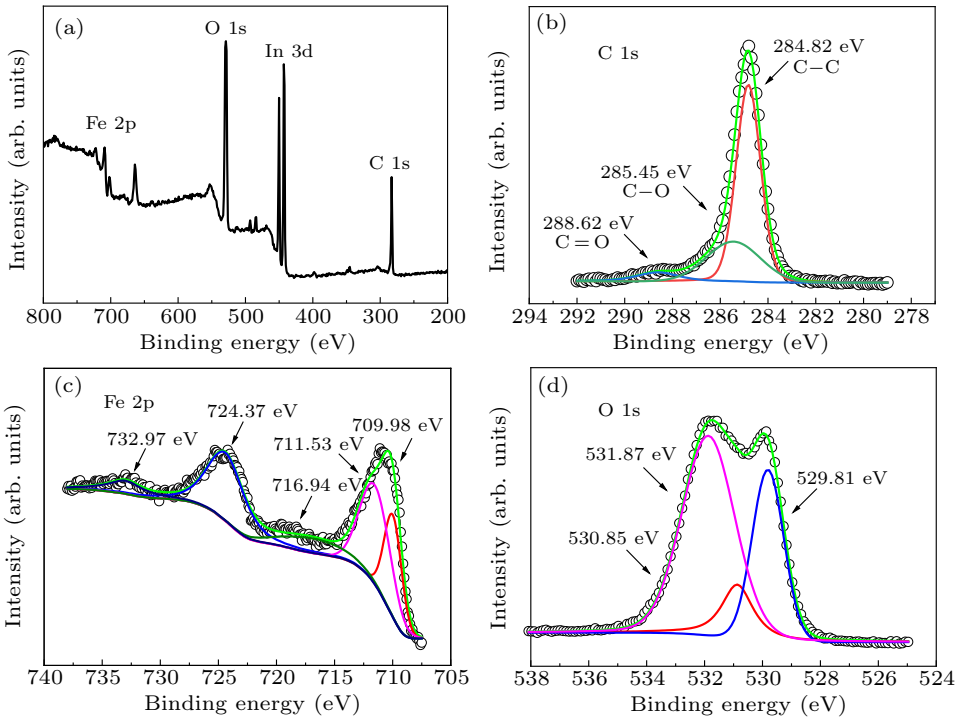


Fig. 4. (a) Survey XPS spectra of the α-Fe_2O_3 nanosheet arrays. (b) C 1s, (c) Fe 2p, and (d) O 1s high resolution XPS spectra of the α-Fe_2O_3 nanosheet arrays.

The XPS measurement has been carried out to identify the surface elemental compositions and chemical states of the as-prepared α-Fe_2O_3 nanosheet arrays, as shown in Fig. 4. Figure 4(a) reveals the survey XPS spectra of the α-Fe_2O_3 nanosheet arrays. It is observed that only the Fe, O, In, and together with the C elements can be found in the surface of the as-prepared α-Fe_2O_3 nanosheet arrays. Usually, a small amount of carbon deriving from the surface carbon-based groups of the samples has been employed as the standard signal source to calibrate the other elements such as the Fe, In, and O elements,[8,27,28] which should result from the XPS instrument itself, as shown in Fig. 4(b). Additionally, the indium element should originate from the ITO substrate. Figure 4(c) indicates the Fe 2p high-resolution XPS spectrum and its Gaussian fitting diagram of the as-prepared sample. It is clearly shown that the Ti 2p core-level spectrum can be decomposed into five Gaussian peaks located at the binding energies of 732.97 eV, 724.37 eV, 716.94 eV, 711.53 eV, and 709.98 eV, respectively. The Gaussian peak appeared at the binding energy of 709.98 eV is corresponding to Fe^{2+},[53,54] while the Gaussian peaks near the binding energies of 724.37 eV and 711.53 eV are associated with Fe $2p_{1/2}$ and Fe $2p_{3/2}$, respectively.[55] Moreover, the distinguishable satellite peaks related to the binding energies of 732.97 eV and 724.37 eV can be observed, which demonstrates the existence of Fe^{3+} in the as-prepared α-Fe_2O_3 nanosheet arrays.[45,51] Figure 4(d) shows the O 1s high-resolution XPS spectrum and its Gaussian fitting diagram of the as-prepared sample. It

is obvious that the O 1s core-level spectrum can be isolated with three Gaussian fitting peaks such as the binding energies of 529.81 eV, 530.85 eV, and 531.87 eV, which are attributed to the Fe–O bonds in the lattice oxygen, oxygen vacancies, and the chemisorbed hydroxyl groups[2,54,56] of the as-prepared sample, respectively. It can be seen from the results above that a significant amount of oxygen vacancies exist in the as-prepared α-Fe_2O_3 nanosheet arrays sample, which have been suggested to be responsible for the nonvolatile resistive switching behavior of the as-prepared W/α-Fe_2O_3/ITO memristor.

Figure 5(a) depicts the UV-visible absorption spectrum of the as-prepared α-Fe_2O_3 nanosheet arrays. It is obvious that the excellent optical absorption property with an absorption edge of about 650 nm corresponding to the indirect optical band gap of about 1.85 eV in the visible absorption region can be observed clearly in the as-prepared α-Fe_2O_3 nanosheet array. Figure 5(b) shows the Tauc plots of the as-prepared α-Fe_2O_3 nanosheet arrays. It is clear that the optical band gap of the as-prepared α-Fe_2O_3 nanosheet arrays can be given with the Tauc relation as given below:[52]

$$(\alpha h\upsilon)^k = A(h\upsilon - E_g), \tag{1}$$

where E_g is the optical band gap of the as-prepared sample, while the α, h, v, A, k are the absorbance coefficient, Planck's constant, vibration frequency, optical constant, and the vibration frequency of the as-prepared sample. As indicated in Fig. 5(b), the optical band gap of the as-prepared α-Fe_2O_3 nanosheet arrays sample is about 1.85 eV, which is lower than that of the intrinsic α-Fe_2O_3[54] (2.1 eV) due to the existence of the intrinsic oxygen vacancies in the as-prepared α-Fe_2O_3 nanosheet arrays. In addition, the lower band gap of the as-prepared α-Fe_2O_3 nanosheet arrays will facilitate decreasing the set and reset voltages of the W/α-Fe_2O_3/ITO memristor, which suggests that the as-prepared W/α-Fe_2O_3/ITO memristor is suitable for the ultralow power nonvolatile memory applications.

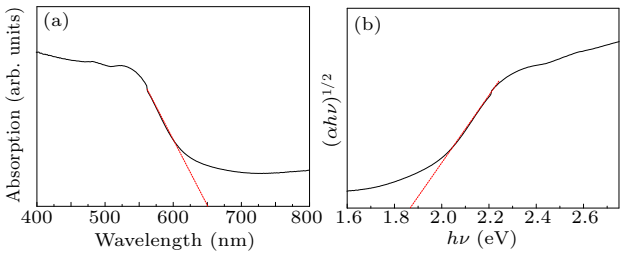


Fig. 5. (a) UV-visible absorption spectrum of the α-Fe_2O_3 nanosheet arrays. (b) Tauc plots of the α-Fe_2O_3 nanosheet arrays.

3.2. Electrical characteristics

Figure 6 records the I–V curve characteristics of the as-prepared α-Fe_2O_3 nanosheet arrays-based W/α-Fe_2O_3/ITO memristor. As shown in Fig. 6(a), the voltage scanning direction is set to 0 V $\rightarrow -1$ V $\rightarrow$ 0 V $\rightarrow +1$ V $\rightarrow$ 0 V. The arrows in Fig. 6(a) indicate the voltage scanning direction, and the numbers represent the voltage scanning sequence. During the test, the bias voltage is always applied to the W top electrode of the device, while the ITO bottom electrode is grounded. To refrain the W/α-Fe_2O_3/ITO memristor from being a permanent breakdown, the compliance current has been set to 10 mA. Figure 6(b) displays the semi-logarithmic I–V curves of the as-prepared W/α-Fe_2O_3/ITO memristor for successive cycles. It is clearly shown that the initial resistance state of the as-prepared W/α-Fe_2O_3/ITO memristor is a high resistance state when the reverse bias voltage is applied.

In the set process, the initial high resistance state of the as-prepared W/α-Fe_2O_3/ITO memristor will be remained until a large enough set voltage (V_{set}) is applied. When the V_{set} reaches -0.6 V, the significant current increase can be observed, indicating that the resistance of the as-prepared W/α-Fe_2O_3/ITO memristor has a dramatic drop from the high resistance state of about 9.8×10^4 Ω to the low resistance state of approximately 1.1×10^2 Ω, and the device switches from the HRS to LRS. When the scanning voltage decreases, the as-prepared W/α-Fe_2O_3/ITO memristor will maintain in the low resistance state until the forward reset voltage (V_{reset}) is applied, indicating the nonvolatile resistive switching characteristics of the as-prepared W/α-Fe_2O_3/ITO memristor. When the forward bias voltage continues to increase until the reset voltage (V_{reset}) is set to 0.7 V, the as-prepared W/α-Fe_2O_3/ITO memristor changes from the LRS to HRS, meaning that the reset process occurs. It can be seen from Figs. 6(a) and 6(b) that the as-prepared W/α-Fe_2O_3/ITO memristor exhibits the nonvolatile bipolar switching characteristics, and the switching ratio (R_{HRS}/R_{LRS}) between the HRS and LRS is approximately three orders of magnitude at the reading voltage of 0.1 V. Figure 6(c) displays the conductance–voltage (C–V) curve of the as-prepared W/α-Fe_2O_3/ITO memristor. It is observed that the stable nonvolatile resistive switching window with a high conductance ratio of about three orders of magnitude can be achieved by sweeping the external voltage in the order of 0 V $\rightarrow -1$ V $\rightarrow$ 0 V $\rightarrow +1$ V $\rightarrow$ 0 V, demonstrating the potential applications of the as-prepared W/α-Fe_2O_3/ITO memristor in the nonvolatile memory devices. To estimate the retention characteristics of the as-prepared W/α-Fe_2O_3/ITO memristor, the reading voltage of 0.1 V has been set to make the device reach the HRS and LRS, respectively. Figure 6(d) shows the retention characteristics of the as-prepared W/α-Fe_2O_3/ITO memristor at the reading voltage of 0.1 V. It is obvious that the R_{HRS}/R_{LRS} between the HRS and LRS is about 10^3, which can be stably maintained and no further degradation occurs even after 1.1×10^3 s. Moreover, the R_{HRS}/R_{LRS} would remain for a longer time from the perspective of development trend. The results show that the W/α-Fe_2O_3/ITO memristor possesses a reliable nonvolatile bipolar resistive switching characteristic. Table 1 tabulates the summary of the Fe_2O_3-based memris-

tors. In comparison with the previous literatures about the α-Fe_2O_3-based memristors,[2,35–38,41,42,45,48,50] the as-prepared α-Fe_2O_3 nanosheet arrays-based W/α-Fe_2O_3/ITO memristor in this work has presented a relatively lower set voltage (-0.6 V) and reset voltage (0.7 V), and the highest resistance ratio of about three orders of magnitude, which demonstrate the promising potential of the as-prepared α-Fe_2O_3 nanosheet arrays-based W/α-Fe_2O_3/ITO memristor for applications in the further ultralow power nonvolatile memory devices.

To illustrate the conduction mechanism of the as-prepared α-Fe_2O_3 nanosheet arrays-based W/α-Fe_2O_3/ITO memristor, the I–V curve of the high resistance state for the W/α-Fe_2O_3/ITO memristor in the set process has been replotted in the $|V|^{1/2}$–ln(I) scale, as shown in Fig. 7. It is clearly shown that the slope of the I–V fitting curve of the as-prepared W/α-Fe_2O_3/ITO memristor is about 2.55 in the high resistance state, suggesting that the resistive switching behavior of the device conforms with the tunneling conduction mechanism modified by the oxygen vacancies. The current density (J) of the high resistance state for the W/α-Fe_2O_3/ITO memristor in the set process can be linearly fitted by the Schottky equation[32,57]

$$J = A^* \times T^2 \times \exp\left[\frac{q\left(\sqrt{\frac{qV}{4\pi\varepsilon d}} - \phi_b\right)}{KT}\right], \tag{2}$$

where A^* is the effective Richardson constant, q is the electrical charge, V is the applied voltage, ε is the dielectric constant, ϕ_b is the Schottky barrier height, K is the Boltzmann's constant, d is the Schottky conduction distance, and T is the absolute temperature.[21]

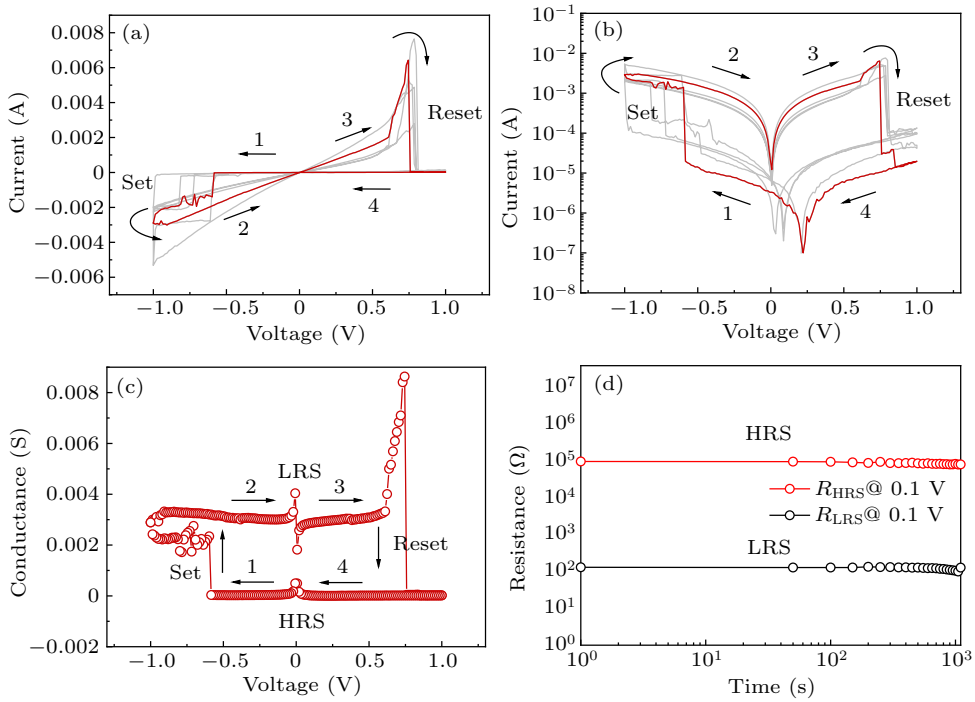


Fig. 6. (a) The linear I–V curves of the W/α-Fe_2O_3/ITO memristor for successive cycles. (b) The semi-logarithmic I–V curves of the W/α-Fe_2O_3/ITO memristor for successive cycles. (c) The C–V curve of the device. (d) The retention characteristics of the device at 0.1 V.

Table 1. Summary of the α-Fe_2O_3-based memristors.

Device structure	V_{set}/V_{reset} (V)	Synthesis process	R_{HRS}/R_{LRS} ratio	Retention	Reference
Top-probe/α-Fe_2O_3/ZnO/bottom-probe	$-0.55/-$	spin coating technique	~ 20	10^3 s	[2]
Au/Fe_2O_3/FTO	$\sim +1.5/\sim -1.2$	ultrasonic spray pyrolysis	~ 10	10 h	[35]
Pt/Fe_2O_3/Pt/Ti	$+1.4/+0.5$	magnetron sputtering technique	~ 7	–	[36]
Ag/Fe_2O_3/ZnO/ITO	$+0.9/-1$	spin coating technique	~ 90.1	30 days	[37]
Au/Pt-Fe_2O_3/Ti	$\sim -1/\sim +3.4$	dip coating method	~ 10	5×10^4 s	[38]
Ag/Fe_2O_3/Ti	$\sim +0.02/-0.1$	spin coating technique	~ 10	3.6×10^3 s	[41]
W/Fe_2O_3 NC film/Pt	$\sim -1.2/\sim +1.6$	dip coating method	$> 10^2$	10^5 s	[42]
Ag/[TiO_2/α-Fe_2O_3]/FTO	$\sim +4/\sim -4$	hydrothermal method	~ 10	10^3 s	[45]
Ti/Pt-Fe_2O_3 core-shell NPs/Pt/PES	$+2.5/-$	hydrothermal method	< 10	–	[48]
Ti/Fe_2O_3-SiO_2/Si	$+2/-2.5$	atomic layer deposition process	2.8	–	[50]
W/α-Fe_2O_3/ITO	$-0.6/+0.7$	hydrothermal method	$\sim 10^3$	$> 10^3$ s	this work

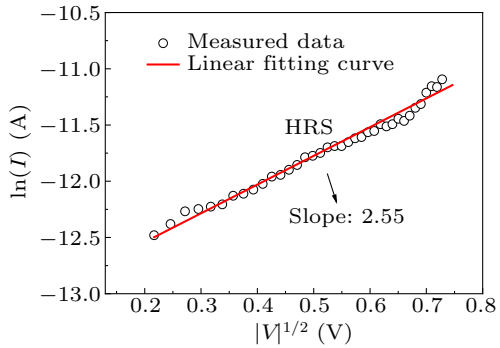


Fig. 7. The I–V curve of the W/α-Fe_2O_3/ITO memristor in the $|V|^{1/2}$–ln(I) scale.

To further clarify the nonvolatile resistive switching mechanism of the as-prepared α-Fe_2O_3 nanosheet arrays-based W/α-Fe_2O_3/ITO memristor, figure 8 reveals the schematic illustration of the corresponding band positions for the α-Fe_2O_3 and ITO before and after the formation of n–n heterojunction under the reverse bias voltage. It has been found that the work function (φ) of α-Fe_2O_3 is 5.88 eV,[2] which is much higher compared with that of the ITO (φ = 4.7 eV) and W (φ = 4.5 eV). Once the formation of the n–n heterojunction occurs at the α-Fe_2O_3/ITO heterojunction interface, the electrons originating from the Fermi energy level (E_F) of the ITO drift toward the α-Fe_2O_3 until the Fermi energy levels on both sides are equal, resulting in raising the energy level of conduction band (E_C) for the α-Fe_2O_3/ITO heterojunction interface. Thus, the nonvolatile bipolar resistive switching behavior of the as-prepared W/α-Fe_2O_3/ITO memristor can be achieved by dominating the energy barrier generated at the α-Fe_2O_3/ITO heterojunction interface.

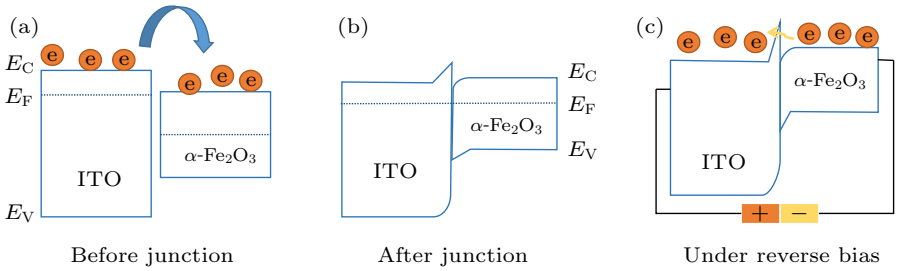


Fig. 8. Schematic illustration of the corresponding band positions for α-Fe_2O_3 and ITO before and after the formation of n–n heterojunction under the reverse bias voltage.

When the reverse bias voltage is set to the as-prepared W/α-Fe_2O_3/ITO memristor, the electrons injected from the α-Fe_2O_3 interface are blocked by the n–n heterojunction at the α-Fe_2O_3/ITO heterojunction interface, leading to a large built-in electric field applying across the depletion layer.[56] By increasing the reverse bias voltage, the high-doping region predominated by the migrating oxygen vacancies get occupied at the α-Fe_2O_3/ITO heterojunction interface would generate in the ITO interface, while the electrons could form another high-doping region in the α-Fe_2O_3 interface. Therefore, the practical depletion layer width and energy barrier decrease apparently with the rising reverse bias voltage. Once the effective barrier layer width becomes significantly thin enough, considerable amounts of electrons stemming from the α-Fe_2O_3 interface would tunnel through the energy barrier and produce the conducting filaments across the α-Fe_2O_3/ITO n–n heterojunction interface,[2] which induce the as-prepared W/α-Fe_2O_3/ITO memristor to transition from the HRS to LRS with a sudden jump of current and the set process occurs. Subsequently, the LRS would be maintained until the forward reset voltage is applied due to the high density of ionic or charged groups across the α-Fe_2O_3/ITO heterojunction interface, indicating the nonvolatile resistive switching behavior of the as-prepared W/α-Fe_2O_3/ITO memristor. In the reset process, the built-in electric field across the α-Fe_2O_3/ITO heterojunction interface would decrease owing to the reverse movement of the occupied charges away from the n–n heterojunction interface when the interface is forward biased, causing a further decrease of the depletion layer and a dramatic rise of the forward current. In addition, a sufficient amount of heat generated by the Joule heating would break the local conducting filaments when the high forward current density injects into the metallic conducting filaments across the α-Fe_2O_3/ITO heterojunction interface,[16] and then the as-prepared W/α-Fe_2O_3/ITO memristor would switch from the LRS to HRS with an abrupt drop of current, demonstrating the nonvolatile bipolar resistive switching behavior of the α-Fe_2O_3 nanosheet arrays-based memristor.

4. Conclusion

In summary, this paper has reported a facile one-step hydrothermal method to prepare synthesize the α-Fe_2O_3 nanosheet arrays with the preferred orientation along the [104] direction on the ITO substrate. The circular W top electrodes have been deposited on the α-Fe_2O_3 nanosheet arrays by magnetron sputtering and the as-prepared α-Fe_2O_3 nanosheet arrays-based W/α-Fe_2O_3/ITO memristor has exhibited a reliable nonvolatile bipolar resistive switching characteristic with the high resistance ratio of about 10^3, good resistance retention over 10^3 s, ultralow set voltage of −0.6 V, and reset voltage of 0.7 V, and good durability. The tunneling conduction mechanism modified by the oxygen vacancies has been proposed, which has been believed to be responsible for

the nonvolatile resistive switching behavior of the as-prepared W/α-Fe_2O_3/ITO memristor. This work suggests that the as-prepared α-Fe_2O_3 nanosheet arrays-based W/α-Fe_2O_3/ITO memristor has been regarded as one promising candidate for further ultralow power nonvolatile memory applications.

Acknowledgements

Project supported by the National Natural Science Foundation of China (Grant Nos. 62341305 and 22269002), the Natural Science Foundation of Guangxi Zhuang Autonomous Region, China (Grant No. 2024GXNSFFA010007), the Science and Technology Project of Guangxi Zhuang Autonomous Region, China (Grant No. AD19110038), the Key Laboratory of AI and Information Processing, Education Department of Guangxi Zhuang Autonomous Region (Grant No. 2024GXZDSY015), and the Innovation Project of Guangxi University of Science and Technology Graduate Education (Grant No. GKYC202408). The authors would like to thank the Shiyanjia Laboratory (www.shiyanjia.com) for the XPS test and XRD refinement.

References

[1] Strukov D B, Snider G S, Stewart D R and Williams R S 2008 *Nature* **453** 80
[2] Sarkar D and Singh A K 2017 *J. Phys. Chem. C* **121** 12953
[3] Yang J J, Pickett M D, Li X M, Ohlberg D A A, Stewart D R and Williams R S 2008 *Nat. Nanotechnol.* **3** 429
[4] Kim S, Lee J, Ling L, Liu S E, Lim H, Sangwan V K, Hersam M C and Lee H 2021 *Adv. Mater.* **34** 2106913
[5] Li J M, Su W X, Li J, Wang L, Ren J, Zhang S, Cheng P T, Hong H, Wang D H, Zhou Y, Mi W B and Du Y W 2021 *Nano Lett.* **21** 5060
[6] Shan X Y, Wang Z Q, Lin Y, Zeng T, Zhao X N, Xu H Y and Liu Y C 2020 *Adv. Electron. Mater.* **6** 2000536
[7] Yu Z Q, Liu M L, Lang J X, Qian K and Zhang C H 2018 *Acta Phys. Sin.* **67** 157302 (in Chinese)
[8] Yu Z Q, Sun T Y, Liu B S, Zhang L, Chen H J, Fan X S and Sun Z J 2021 *J. Alloys Compd.* **858** 157749
[9] Alam M W, Jamir A, Longkumer B, Souayeh B, Sadaf S and Moirangthem B 2025 *J. Alloys Compd.* **1010** 177032
[10] Huang C, Chang W, Huang J, Lin S and Chueh Y 2017 *Nanoscale* **9** 6920
[11] Ismail M, Mahata C, Kang M and Kim S 2023 *Ceramics International* **49** 19032
[12] Qi Y F, Shen Z J, Zhao C and Zhao C Z 2020 *J. Alloys Compd.* **822** 153603
[13] Carvalho R C, Betts A J and Cassidy J F 2020 *Phys. Chem. Chem. Phys.* **22** 4216
[14] Sun Y M, Song C, Yin J, Qiao L L, Wang R, Wang Z Y, Chen X Z, Yin S Q, Saleem M S, Wu H Q, Zeng F and Pan F 2019 *Appl. Phys. Lett.* **114** 193502
[15] Kyesmen P I, Nombona N and Diale M 2021 *ACS Omega* **6** 33398
[16] Liang K D, Huang C H, Lai C C, Huang J S, Tsai H W, Wang Y C, Shih Y C, Chang M T, Lo S C and Chueh Y L 2014 *ACS Appl. Mater. Interfaces* **6** 16537
[17] Huang C H, Matsuzaki K and Nomura K J 2020 *Appl. Phys. Lett.* **116** 023503
[18] Cui D S, Du Y W, Lin Z H, Kang M Y, Wang Y F and Su J 2021 *IEEE Electron Dev. Lett.* **44** 237
[19] Almadhoun M N, Speckbacher M, Olsen B C, Luber E J, Sayed S Y, Tornow M and Buriak J M 2021 *Nano Lett.* **21** 2666
[20] Persson K, Ram M S, Kilpi O, Borg M and Wernersson L 2020 *Adv. Electron. Mater.* **6** 2000154
[21] Wu S J, Wang F, Zhang Z C, Li Y, Han Y M, Yang Z C, Zhao J S and Zhang K L 2018 *Chin. Phys. B* **27** 087701
[22] Sokolov A S, Jeon Y, Kim S, Ku B, Lim D, Han H, Chae M G, Lee J, Ha B G and Choi C 2018 *Appl. Surf. Sci.* **434** 822
[23] Tu M L, Lu H P, Luo S W, Peng H, Li S D, Ke Y Z, Yuan S G, Huang W, Jie W J and Hao J H 2020 *ACS Appl. Mater. Interfaces* **12** 24133
[24] Li Z H, Li J C and Cui H P 2020 *J. Alloys Compd.* **858** 158091
[25] Kwon D, Kim K M, Jang J H, Jeon J M, Lee M H, Kim G H, Li X, Park G, Lee B, Han S, Kim M and Hwang C S 2010 *Nat. Nanotechnol.* **5** 148
[26] Yu Z Q, Xu J M, Han X, Chen C, Qu X R, Tang J, Sun Z J and Xu Z M 2024 *Mater. Rep.* **38** 23020160
[27] Yu Z Q, Qu X P, Yang W P, Peng J and Xu Z M 2016 *J. Alloys Compd.* **688** 37
[28] Yu Z Q, Qu X P, Yang W P, Peng J and Xu Z M 2016 *J. Alloys Compd.* **688** 294
[29] Liu H C, Tang X G, Liu Q X, Jiang Y P, Li W H, Guo X B and Tang Z H 2020 *Ceramics International* **46** 21196
[30] Huang T T, Tao J C, Xu P R, Yang W L, Niu L K, Chen Z M, Chen X and Dai N 2024 *ACS Appl. Electron. Mater.* **6** 1475
[31] Zhang F, Zhang Y, Li L L, Mou X, Peng H N, Shen S C, Wang M, Xiao K H, Ji S H, Yi D, Nan T X, Tang J S and Yu P 2023 *Nat. Commun.* **14** 3950
[32] Lin C, Wang S, Lee D and Tseng T 2008 *Journal of the Electrochemical Society* **155** H615
[33] Yu Z Q, Jia J H, Ou M L, Sun T Y and Xu Z M 2025 *Chin. Phys. B* **34** 127302
[34] Ismail M, Mahata C, Kang M and Kim S 2023 *Ceramics International* **49** 19032
[35] Yan X B, Li Y C, Zhao J H, Xia Y D, Zhang M L and Liu Z G 2015 *Phys. Lett. A* **379** 2392
[36] Inoue I H, Yasuda S, Akinaga H and Takagi H 2008 *Phys. Rev. B* **77** 035105
[37] Khan M U, Hassan G and Bae J 2020 *Journal of Materials Science: Materials in Electronics* **31** 1105
[38] Hu Q L, Park M, Shim J H, Yoon T, Choi Y J and Kang C J 2014 *Microelectronic Engineering* **127** 40
[39] Yoo E J, Kang S Y, Shim E L, Yoon T S, Kang C J and Choi Y J 2015 *J. Nanosci. Nanotechnol.* **15** 8622
[40] Zhou G D, Wu B, Liu X Q, Li Z L, Zhang S J, Zhou A K and Yang X D 2016 *J. Alloys Compd.* **678** 31
[41] Ren Z J, Zhou G D and Wei S Q 2020 *Phys. Chem. Chem. Phys.* **22** 2743
[42] Ko Y, Ryu S W and Cho J 2016 *Appl. Surf. Sci.* **368** 36
[43] Zhao W X, Li Q L, Sun B, Shen Z, Liu Y H and Chen P 2014 *Solid State Commun.* **194** 16
[44] Nguyen H H, Ta H K T, Park S, Phan T B and Pham N K 2010 *RSC Adv.* **10** 12900
[45] Sun B, Li Q L, Zhao W X, Li H W, Wei L J and Chen P 2014 *J. Nanopart. Res.* **16** 2389
[46] Sun B, Liu Y H, Zhao W X and Chen P 2015 *RSC Adv.* **5** 13513
[47] Lee J Y, Kim J, Baek Y, Choi Y J, Kang C J, Lee H H and Yoon T 2014 *Appl. Phys. Lett.* **104** 093514
[48] Baek Y, Hu Q L, Yoo J W, Choi Y J, Kang C J, Lee H H, Min S, Kim H, Kim K and Yoon T 2013 *Nanoscale* **5** 772
[49] Lee J, Baek Y, Hu Q L, Choi Y J, Kang C J, Lee H H, Kim H, Kim K and Yoon T 2013 *Appl. Phys. Lett.* **102** 122111
[50] Kukli K, Kemell M, Castán H, Dueñas S, Link J, Stern R, Heikkilä M J, Jõgiaas T, Kozlova J, Rähn M, Mizohata K, Ritala M and Leskelä M 2020 *J. Vac. Sci. Technol. A* **38** 042405
[51] Chong R F, Du Y Q, Chang Z X, Jia Y H, Qiao Y, Liu S H, Liu Y, Zhou Y M and Li D L 2019 *Applied Catalysis B: Environmental* **250** 224
[52] Liu J, Cai Y Y, Tian Z F, Ruan G S, Ye Y X, Liang C H and Shao G S 2014 *Nano Energy* **9** 282
[53] Yan W J, Zeng X M, Liu H, Guo C W, Ling M and Zhou H P 2019 *Chin. Phys. B* **28** 106801
[54] Zhang J, Zhu G Q, Liu W G, Xi Y X, Golosov D A, Zavadski S M and Melnikov S N 2020 *J. Alloys Compd.* **834** 154992
[55] Wu Q N, Meng D D, Zhang Y, Zhao Q D, Bu Q J, Wang D J, Zou X X, Lin Y H, Li S and Xie T F 2019 *J. Alloys Compd.* **782** 943
[56] Zhang P, Gao C X, Lv F Z, Wei Y P, Dong C H, Jia C L, Liu Q F and Xue D S 2014 *Appl. Phys. Lett.* **105** 152904
[57] Chabungbam A S, Thakre A, Kim D, Kim M, Kim G, Lee H and Park H 2024 *Appl. Surf. Sci.* **670** 160681